EUMETSAT Satellite Application Facility on Climate Monitoring

Algorithm Theoretical Basis Document

FTH release 1.0

DOI: 10.5676/EUM_SAF_CM/FTH_METEOSAT/V001

Free Tropospheric Humidity **CM-139**

Reference Number:	SAF/CM/DWD/ATBD/FTH/1.2
Issue/Revision Index:	1.2
Date:	10.12.2012

Document Signature Table

	Name	Function	Signature	Date
Author	Marc Schröder Remy Roca	CM SAF scientist LMD scientist		10/12/2012
Editor	Rainer Hollmann	Science Coordinator		
Approval	Rainer Hollmann	Science Coordinator		
Release	Martin Werscheck	Project Manager		

Distribution List

Internal Distribution	
Name	**No. Copies**
DWD Archive	1
CM SAF Team	1

External Distribution		
Company	**Name**	**No. Copies**
PUBLIC		1

Document Change Record

Issue/ Revision	Date	DCN No.	Changed Pages/Paragraphs
1.1		SAF/CM/DWD/ATBD/FTH	First version after check point meeting
1.2		SAF/CM/DWD/ATBD/FTH	DRI7 RIDs implemented

Applicable documents

Reference	Title	Code
AD 1	Memorandum of Understanding between CM SAF and LMD, Paris, France	

Reference documents

Reference	Title	Code
RD 1	CM SAF Product Requirements Document	SAF/CM/DWD/PRD/2.0

Table of Contents

List of Figures

List of Tables

1 The EUMETSAT SAF on Climate Monitoring

The importance of climate monitoring with satellites was recognized in 2000 by EUMETSAT Member States when they amended the EUMETSAT Convention to affirm that the EUMETSAT mandate is also to “contribute to the operational monitoring of the climate and the detection of global climatic changes". Following this, EUMETSAT established within its Satellite Application Facility (SAF) network a dedicated centre, the SAF on Climate Monitoring (CM SAF, http://www.cmsaf.eu).
The consortium of CM SAF currently comprises the Deutscher Wetterdienst (DWD) as host institute, and the partners from the Royal Meteorological Institute of Belgium (RMIB), the Finnish Meteorological Institute (FMI), the Royal Meteorological Institute of the Netherlands (KNMI), the Swedish Meteorological and Hydrological Institute (SMHI), the Meteorological Service of Switzerland (MeteoSwiss), and the Meteorological Service of the United Kingdom (UK MetOffice). Since the beginning in 1999, the EUMETSAT Satellite Application Facility on Climate Monitoring (CM SAF) has developed and will continue to develop capabilities for a sustained generation and provision of Climate Data Records (CDR’s) derived from operational meteorological satellites.
In particular the generation of long-term data sets is pursued. The ultimate aim is to make the resulting data sets suitable for the analysis of climate variability and potentially the detection of climate trends. CM SAF works in close collaboration with the EUMETSAT Central Facility and liaises with other satellite operators to advance the availability, quality and usability of Fundamental Climate Data Records (FCDRs) as defined by the Global Climate Observing System (GCOS). As a major task the CM-SAF utilizes FCDRs to produce records of Essential Climate Variables (ECVs) as defined by GCOS. Thematically, the focus of CM SAF is on ECVs associated with the global energy and water cycle.

Another essential task of CM SAF is to produce data sets that can serve applications related to the new Global Framework of Climate Services initiated by the WMO World Climate Conference-3 in 2009. CM SAF is supporting climate services at national meteorological and hydrological services (NMHSs) with long-term data records but also with data sets produced close to real time that can be used to prepare monthly/annual updates of the state of the climate. Both types of products together allow for a consistent description of mean values, anomalies, variability and potential trends for the chosen ECVs. CM SAF ECV data sets also serve the improvement of climate models both at global and regional scale.
As an essential partner in the related international frameworks, in particular WMO SCOPE-CM (Sustained COordinated Processing of Environmental satellite data for Climate Monitoring), the CM SAF - together with the EUMETSAT Central Facility, assumes the role as main implementer of EUMETSAT’s commitments in support to global climate monitoring. This is achieved through:

- Application of highest standards and guidelines as lined out by GCOS for the satellite data processing,
- Processing of satellite data within a true international collaboration benefiting from developments at international level and pollinating the partnership with own ideas and standards,
- Intensive validation and improvement of the CM SAF climate data records,
- Taking a major role in data set assessments performed by research organisations such as WCRP. This role provides the CM SAF with deep contacts to research organizations that form a substantial user group for the CM SAF CDRs,
- Maintaining and providing an operational and sustained infrastructure that can serve the community within the transition of mature CDR products from the research community into operational environments.

A catalogue of all available CM SAF products is accessible via the CM SAF webpage, www.cmsaf.eu/. Here, detailed information about product ordering, add-on tools, sample programs and documentation is provided.

2 Introduction

This CM SAF Algorithm Theoretical Basis Document (ATBD) provides information on the algorithms implemented for the homogenisation of METEOSAT clear sky radiances and the retrieval of free tropospheric humidity (CM-139, FTH_MVIRI) using ECMWF reanalysis and cloud cover as well as cloud top pressure information from ISCCP-DX. MVIRI observations from METEOSAT 2-7 (ISCCP-DX) and SEVIRI (DWD archive) observations from METEOSAT8-9 are employed. The retrieved products have a spatial and temporal resolution of 0.625° and 3 hours, respectively.

Laboratoire Météorologie Dynamique (LMD) has developed a retrieval algorithm to convert raw clear sky radiances of the 6.3 μm channel of Meteosat First Generation (MFG, METEOSAT2-7) into the free tropospheric humidity (FTH) product (Roca et al., 2003; Brogniez et al., 2004; Roca et al., 2011). Also work on the construction of the clear sky radiance archive over the period 1983-1997 with special emphasis on the temporal homogeneity of the final database (Picon et al., 2003) has been carried out. Clear sky was defined using the ISCCP-DX data set. LMD has finished the production of the FTH and clear sky radiance data set for MFG with a temporal sampling of 3 hours and a spatial resolution of 0.625° for the period 1983-2005 for the nominal position.

Within a Research and Operation activity the retrieval and homogenization developments at LMD were transferred into the environment at CM SAF in order to sustain and increase the availability of long temporal records related to atmospheric humidity at CM SAF. Also in close cooperation with LMD the time series could be extended into the SEVIRI period and covers now the period July 1983 to December 2009 (Roca et al., 2009; Roca et al., 2012).

CM SAF activities related to the generation of the FTH data set from MVIRI and SEVIRI observations were part of a pilot project within the Sustained, Coordinated Processing of Environmental Satellite Data for Climate Monitoring (SCOPE-CM). The aim of the SCOPE-CM is to establish a network of facilities ensuring continuous and sustained provision of high-quality satellite products related to the Essential Climate Variables (ECV), on a global scale, responding to the requirements of the Global Climate Observing system (GCOS).

The document gives background information on the physics of the problem, the training and derivation of the statistical inversion scheme and consideration of constraints and limitations of the retrieval. It is based on Picon et al. (2003) and a working contract report between LMD and CM SAF (Roca et al., 2009; Roca et al., 2012).

The FTH processing software as implemented at DWD (for an overview see Figure 5-1) is the property of CNRS and CM SAF/DWD.

At first a description of the data sources and an introduction to the homogenization method for the MVIRI and SEVIRI radiometers is given, followed by a description of the retrieval scheme. A series of sensitivity studies is presented and finally, assumptions and limitations are discussed.

More information on the data set is contained in the product requirements document [RD 1].

3 Input data and external software

This section describes the input data sets required for the retrieval of FTH.

Radiance observations and data sets

The Meteosat Visible and Infrared Imager (MVIRI) is a three channel imaging radiometer flown consecutively on Meteosat-2 to Meteosat-7 from the first generation of Meteosat satellites. It observes the Earth from a geostationary orbit at 0° latitude orbit every 30 minutes between 1982 and 2006. The spatial sampling distance of the observations is approximately 5 km at nadir and increases with distance from subsatellite point.
The Spinning Enhanced Visible and Infrared Imager (SEVIRI) carries out observations at 12 channels which cover the visible and thermal infrared spectral wavelength range. SEVIRI is on board Meteosat-8 and -9 (Meteosat second generation), which is a geostationary satellite at 0° latitude. SEVIRI full disc observations are repeated every 15 minutes between 2004 and present. The spatial sampling distance of brightness temperature (BT) observations is 3 km, again increasing with distance from subsatellite point.
The elaboration of the Meteosat clear sky radiance (CSR) archive is described at length in Brogniez et al. (2006, 2009). The archive contains observations of the Africa/tropical Atlantic atmosphere by the first generation of the Meteosat satellites. The 6.3 µm BTs, together with cloud cover and cloud top pressure are taken from the International Satellite cloud Climatology Project (ISCCP; Rossow and Schiffer, 1999) at a 3 hourly time step and an equivalent resolution of 30 km (DX level). The CSR are obtained using the scene selection methodology described in Brogniez et al. (2006, 2009) and based on the ISCCP-DX cloud products: in a regular 0.625° mesh, in addition to the clear-sky only pixels, low-level clouds with a cloud-top pressure greater than 680 hPa are kept in the mesh, improving significantly the sampling of the region over a season (see Brogniez et al. (2006) for details). Thus, the radiances are not cloud clarified and original radiance observations are utilised. All observations are adapted to Meteosat-5 spectral response function (for Meteosat-8/9 adaptation see Roca et al., 2009). The LMD CSR archive is homogenised following the approach described in Picon et al. (2003). Note that the intercalibration to HIRS (Breon et al., 2000) can optionally be applied to the CSR data as long as Meteosat-5 is considered as reference. When applied, the result is consistent with HIRS channel 12 observations on NOAA12. The CSR archive from LMD, with Meteosat-5 as reference, is utilised as input and covers the 17th July 1983 – June 2005 period.

For the period July 2005 – June 2006 ISCCP-DX data is used and processed as described above, except for July 2005 for which the normal calibration was removed following a recommendation from ISCCP and applying coefficients provided by ISCCP.

For July 2006 onwards SEVIRI observations in sensor resolution from DWD archive are used. They are sampled to mimic ISCCP-DX radiance data. Cloud information is taken from ISCCP and further approaches are described in Brogniez et al. (2006).

Reanalysis

The training database for the estimation of the regression coefficients a and b (see section 5.1) needs to be representative of the atmospheric states encountered over the area of study. Section 5.2 discusses the effect of the training area on the retrieval. The training database is composed of temperature (T) and specific humidity (q) profiles extracted from the ECMWF reanalyses ERA-Interim (Dee et al., 2010). ERA Interim is available at 6-hourly resolution and a horizontal grid in 0.75º resolution. The ERA Interim training database is composed of clear sky only profiles covering the years 2001, 2006 and 2007 and sampling the seasonal cycle with the 1st day of the months of January, April, July and October of each

year (4 time steps per day). The clear sky is defined using the ERA Interim cloud fraction with a strict value of 0 at all levels. In addition to the cloud screening, a quality check is also performed on the relative humidity profiles (determined with respect to the water phase only) to remove the driest cases where the relative humidity reaches values below 1% in the free troposphere, and also to remove the saturated profiles (>100%).

ERA-Interim is also used for the determination of homogenisation coefficients (see section 4).

ERA Interim and ERA-40 (Uppala et al., 2005) data is used to determine the thermal parameter p0 (see section 5.1). ERA-40 is available on a 1.125º horizontal grid and with a 6 hourly resolution (0, 6, 12, 18 UTC). Both reanalysis data sets are available on sigma hybrid model levels (ML) and standard pressure levels (PL). Roca et al. (2009) demonstrated that the vertical resolution does not affect FTH quality significantly as long as a certain minimum number of pressure levels is present. 37 pressure levels from ERA Interim are sufficient while the 23 pressure levels from ERA40 are not.

For the period 1983 – 2005 p0 was provided by LMD while for 2006 onwards p0 was computed at DWD.

Adaptation of spectral response functions

The spectral response function adaptations between MET5 and MET8/9 are described in Roca et al. (2009). Scatterplots of simulated MET5 and MET8 as well as MET5 and MET9 exhibit excellent linear behaviour so that a linear equation with slope a and intercept b can be used for adaptation. For completeness the coefficients are repeated here: MET5/MET8 with a=1.0160 and b=-2.3498 and MET5/MET9 with a=1.0174 and b=-2.6033.

Radiative transfer

The simulations of the WV BTs are performed using the version 9.3 of the RTTOV fast radiative code (Radiative Transfer for the TIROS Operational Vertical Sounder, Matricardi et al., 2004). This model, initially developed for the assimilation of TOVS radiances in the ECMWF forecast model, allows the simulation of several other radiometers such as the First Generation of METEOSAT Visible and InfraRed Imager (MVIRI) and the recent Spinning Enhanced Visible and InfraRed Imager (SEVIRI) onboard the METEOSAT Second Generation series. It uses fast transmittance algorithms based on accurate transmittances obtained by line-by-line computations (GENLN2 for the 3-20µm spectral range, Edwards (1992)), and is thus dependent on the spectroscopic database (HITRAN-2000, Rothman et al. (2003)) behind the line-by-line simulations. For the specific case of the 6.3µm strong vibration-rotation absorption band by water vapor, the RTTOV model takes into account the two types of the water vapor continuum (foreign-broadening and self-broadening, model CKD-2.4, Clough et al. (1989)) that has a non-negligible contribution in the water vapor band, and that has been shown to be of the same order of magnitude than calibration uncertainties (~2 K, e.g. Stephens et al. (1996), Soden et al. (2000)). In addition to the fast simulation of the brightness temperatures (BTs), RTTOV also computes the full Jacobian matrices ($\partial BT/\partial X$, where X is any atmospheric parameter), specifically designed for variational assimilation, and particularly useful for the present work to determine the local Jacobian $\partial BT/\partial RH$.

4 Homogenisation approach

Mainly due to satellite changes and changes in calibration the METEOSAT time series is not homogeneous. E.g., changes in vicarious calibration can appear in the time series as jumps. Such jumps can be eliminated using homogenisation approaches. The homogenisation applied here largely follows the work of Picon et al. (2003) which is briefly summarised here.

The basic approach is to utilise ERA Interim data as input to RTTOV9.3 simulations of MET5 observations, to simulate MET5-like BT and apply linear regression to the observed CSR for a month prior and after the jump. Output from the regression is used to modify the satellite observed BT such that bias and RMS between observed and simulated BT are preserved. The underlying assumption is stability of ERA Interim simulations over two months. In order to carry out the comparison the following criteria have been applied:

- Only data at 6 and 12 UTC have been considered.
- Simulations are performed in clear sky only. This is further constrained by considering the warmest 80% in simulated radiances only.
- The subdomain covers ±45°N/S and ±45°E/W.

After double application of the linear regression and substituting for simulated BT the following equation is used to modify CSR prior to the jump:

$$\begin{aligned} \mathrm{BT}_{\mathrm{corrected}} &= \frac{a_{before}}{a_{after}} BT_{original} + b_{before} - b_{after} \frac{a_{before}}{a_{after}} \\ &= a' BT_{original} + b' \end{aligned} \qquad (1)$$

This approach is applied to homogenise the change in calibration in January 2001, the MET7 / MET8 and MET8 / MET 9 transition using ERA Interim data for the months December 2000 and January 2001, June and July 2006, and April and May 2007, respectively, at CM SAF. The following parameters are applied:

- January 2001 onwards: a'=0.98908 and b'=2.10135.
- July 2006 onwards: a'=1.01510 and b'=1.00681
- May 2007 onwards: a'=0.974119 and b'=5.31705.

GSICS results for May to December 2008 exhibit a difference in bias between MET8 and MET9 relative to IASI of slightly less than 0.5 K. Note that this bias is significantly smaller in 2009 and onwards.

In May 2000 the vicarious calibration has been replaced with the calibration using the onboard black body, and an updated version has been implemented in January 2001 (http://www.eumetsat.int/groups/ops/documents/document/pdf_ten_blackbody-calibration.pdf). In parallel the eclipse of the years 2000 and 2001 affected the overall performance (Köpken, 2001). Finally note a series of gain changes, in particular also on 09 January 2001 (http://www.eumetsat.int/groups/ops/documents/document/pdf_rep_gains_hist_met7.pdf).

5 Algorithm description

The non-linear relation between radiation, in particular outgoing longwave radiation, and free tropospheric humidity FTH (elsewhere the term upper tropospheric humidity, UTH is used) explains the large interest of climate scientists in free tropospheric humidity. The commonly applied relationship between brightness temperature and FTH was developed by Soden and Bretherton (1993) for geostationary satellite observations and relies on the assumptions of random strong line theory and constant lapse rate. It was shown that the observed BT is proportional to the logarithm of the mean relative humidity (RH). Under the given assumptions it means that the observed BT is mainly a function of RH alone and not of temperature and specific humidity.

Based on their work, Roca et al. (2003) determined the regression coefficients statistically and used reanalyses to determine the scaled reference pressure while Schmetz et al. (1995) uses reanalyses to determine regression coefficients on pixel basis. Exemplary FTH retrievals based on observations from polar orbiting satellites are described in Buehler and John (2005) for AMSU-B and in Shi and Bates (2011) for HIRS using similar relations but somewhat adapted methods from Soden and Bretherton (1993). Here, the temporal sampling is limited and the time series is affected by orbital drift. The polar and geostationary FTH products can be retrieved under clear sky and low level cloud conditions only.

Jackson and Bates (2001) assessed free tropospheric humidity algorithms applicable to HIRS observations at 6.7 μm. Among other things they concluded that the averaging kernel has a significant effect on the FTH retrieval and that the consideration of p0 in the retrieval improves results in the tropics.

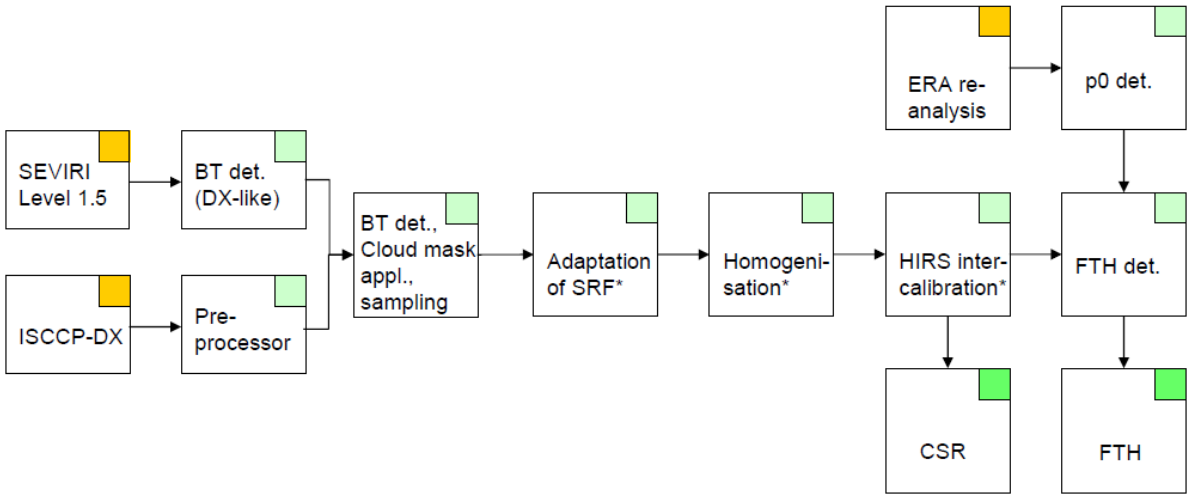

Figure 5-1: *Flow chart for the FTH product. Input data is marked orange, products are marked green and software is marked blue (det.: determination, appl.: application, *: application of predefined coefficients).*

An overview of the FTH computation together with output data and required input data is given in Figure 5-1. Large parts of the processing rely on modifications of BT input and have been described in the previous section, together with a description of the input data. All software modules (marked green in) are the property of CNRS and CM SAF.

After application of the intercalibration to HIRS (Breon et al., 2000), the CSR is consistent with HIRS channel 12 observations on NOAA12.

In the following the conversion of BT into FTH ("FTH det." In Figure 5-1) is discussed in more detail.

5.1 Retrieval scheme

The Free Tropospheric Humidity (FTH) is determined from the following equation, analytically determined by Soden and Bretherton (1993, 1996):

$$\ln\left(\frac{\langle RH\rangle\ p_0}{\cos\theta}\right) = a \times BT_{6.3\mu m} + b \qquad (1)$$

This equation links the clear sky brightness temperature (BT) of a 6.3 µm channel to the mean relative humidity (RH, in % defined with respect to water only) of a broad layer of the troposphere. In the following the free troposphere corresponds to the 700-150 hPa region of the atmosphere. This equation also makes use of a scaling parameter p_0 (see Eq. (2)) and of a correction of the satellite viewing angle θ.

According to the related bibliography, the vertical averaging operator <•> can be:

- The local relative humidity Jacobian $\partial BT/\partial RH$ (e.g. Roca et al., 2003; Brogniez, 2004; Brogniez et al., 2004).
- An idealized Jacobian $\Delta BT/\Delta RH$ whose weights are defined in temperature coordinates (e.g. Soden and Bretherton, 1993; Soden and Bretherton, 1996; Jackson and Bates, 2001).
- The transmission-derived weighting function $\partial\tau/\partial \ln p$ (e.g. Schmetz and Turpeinen, 1988; Stephens et al., 1996).

The fitting parameters (a and b) of the BT-to-<RH> retrieval are determined once using a representative dataset of thermodynamic profiles and sampling the satellite field of view. Implemented are a=-0.1248 and b=33.46 as determined in Roca et al. (2009) and briefly recalled in section 5.2.

The thermal parameter p_0 is defined from the temperature profile as follows:

$$p_0 = \frac{p[T = 240\ K]}{300\ hPa} \qquad (2)$$

.

It represents the deviation from a standard tropical profile where the 240-K isotherm is located at 300 hPa (see Soden and Bretherton (1993) theory).

5.2 Error budget estimates

This section discusses the uncertainty budget estimate for the FTH product. The uncertainty budget is composed of three main uncertainty source terms: 1) calibration uncertainty, 2) retrieval uncertainty and 3) sampling uncertainty.

We consider an upper bound calibration uncertainty of 1 K. In this case, the relative uncertainty on FTH is equivalent to the intercept of the retrieval (b in Eq. (1)) and is between 10 and 15% (van de Berg et al., 1995; Roca et al., 2009). In line with Roca et al. (2010) the calibration uncertainty is considered to be a systematic difference. Retrieval and sampling

uncertainties cause systematic differences and variance and therefore affect accuracy and precision. The primary goal of the training is the determination of the regression coefficients. However, this process also allows an estimation of the retrieval uncertainty. Based on the tropical training RMS=2%RH (8% when assuming an average FTH of 25%) and an average relative difference of 0.3%RH were estimated. Assuming a daily average over a 2.5° grid box and a typical standard deviation of 20% would yield a 10% relative sampling uncertainty. As a result, in this idealized case, the total uncertainty on the FTH mean is driven equally by the calibration and sampling terms and less so by the algorithm term. The estimated total error S is the square root of the square sums and in this case is around 16-19% at one sigma (Roca et al., 2012).

The above uncertainty budgets need to be considered as estimates because they rely on upper boundary uncertainty estimates, on training data basis which might not be fully representative for true variability and on simplifications related to the sampling.

6 Practical Considerations

a) Choice of vertical averaging operator

A detailed analysis on the choice of the vertical operator used to estimate the FTH from the relative humidity profile has been performed at LMD during the elaboration of the first METEOSAT FTH long-term archive (see Brogniez 2004; Brogniez et al., 2004; Roca et al., 2011 - to be submitted to JGR-).

Figure 6-1 illustrates the impact of each weighting function evocated in the related literature (see also previous section) on the relationship of eq. (1) and highlights the better quality of the fit obtained when using the local relative humidity Jacobian J_{RH}. See Roca et al. (2011) for details.

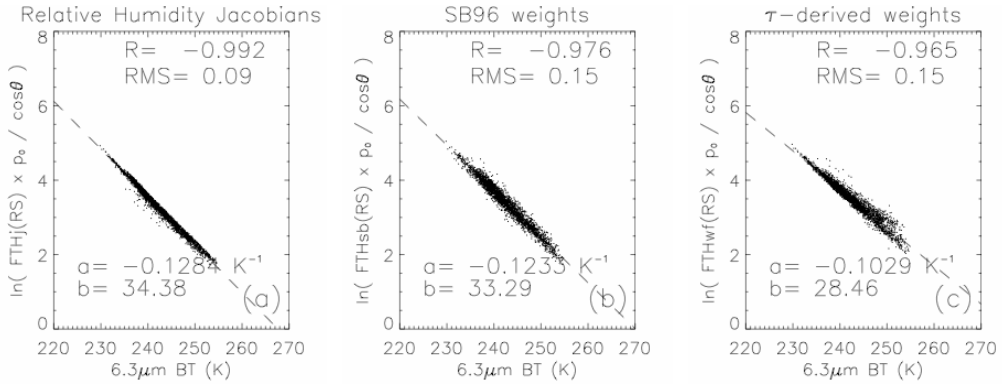

Figure 6-1*: Scatter plots of synthetic 6.3µm BT versus the logarithmic relationship of eq. (1). The theoretical FTH is computed from relative humidity profiles weighted by (a) the relative humidity Jacobian J_{RH}, (b) the Soden and Bretherton (1996) weights and (c) the transmission-derived weighting function τ-WF. The dashed line represents the linear fit used to determine the (a,b) coefficients of eq. (1). The Pearson correlation (R) and the root-mean-square error (RMS) are indicated. From Roca et al. (2011).*

To study the variability of the weighting operators (J_{RH}, SB96 and WF), two parameters are used to describe them for each time step and each grid point:

- The pressure at the maximum of the function.
- The half-width (in hPa) of the layer.

The weighting operators are computed using ERA-40 profiles, together with the RTTOV radiative code (for J_{RH} and WF).

The summer and winter climatologies of the mean pressure of the maximum of the functions for the period 1999-2001 are presented in Figure 6-2. Because of the specific definition of the SB96 (the weights are defined on isotherms) the spatial variability of the function follows the one of the temperature and does not show the patterns highlighted by the BT fields (not shown).

On the opposite, both J_{RH} and WF have their maximum of contribution that follows the water vapour BT patterns, with peaks in the upper levels of the troposphere (~260-340 hPa) in the low BT regions and in the middle troposphere (~400 hPa down to 580 hPa) in the high BT regions.

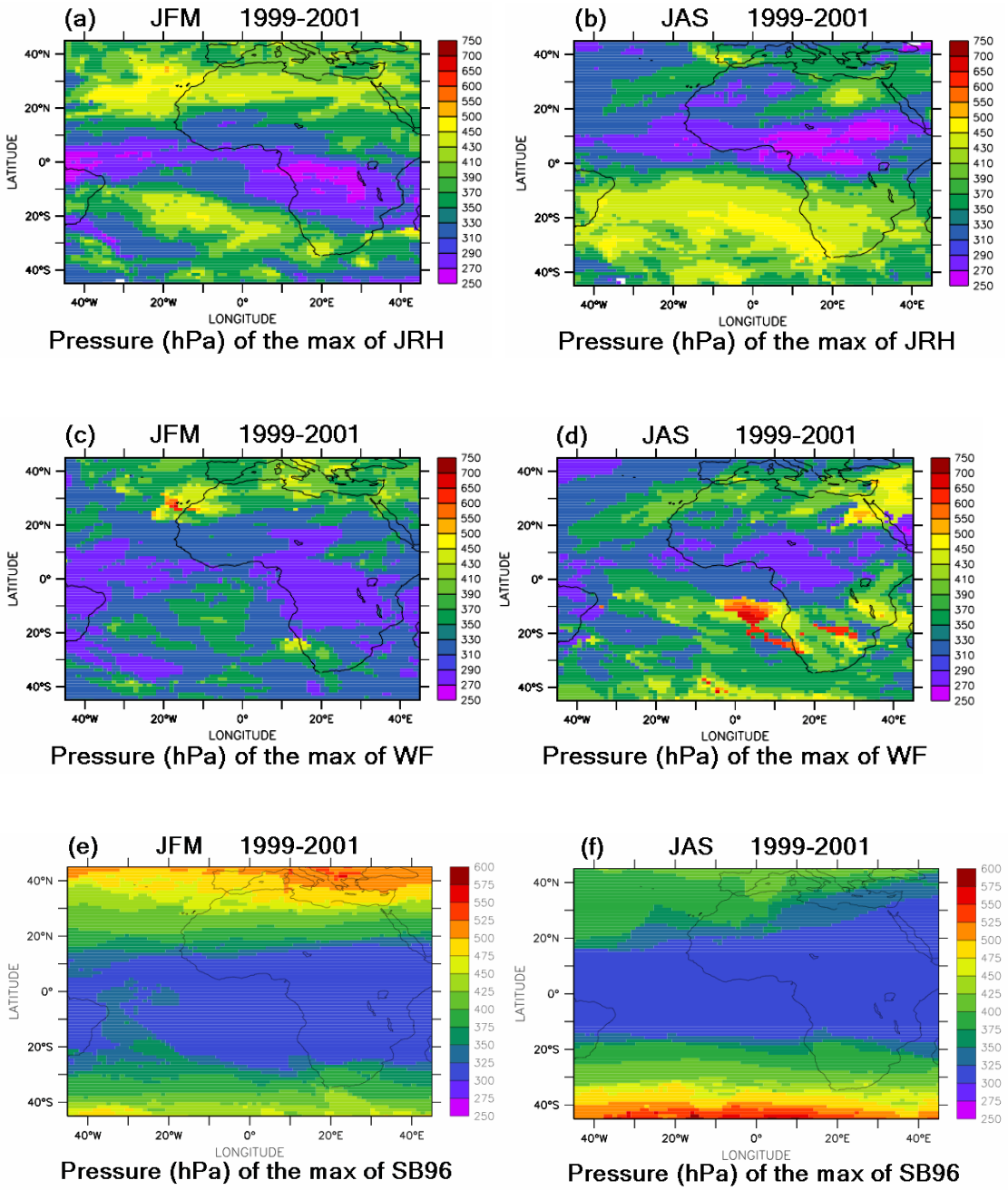

Figure 6-2*: 3-years means (July, August, September - JAS, left, and January, February, March - JFM, right) of the pressure in hPa of the maximum of the three weighting operators: (upper line: a & b) the J_{RH} function, (middle line: c & d) the WF function and (bottom line: e & f) the SB96 function. The climatologies are for clear and low-level clouds scenes.*

This behaviour is clearly explained by the height of contribution of measurements performed in the 6.3µm water vapor absorption band. Indeed in this band, the BT measurement is dominated by the vertical distribution of RH, with a maximum of absorption (low BT) being reached in the upper levels of the troposphere in a moist atmosphere while it is reached in lower levels for a dry atmosphere (high BT).

Although the large-scale structures are similar between the J_{RH} and WF operators, some differences are nevertheless noticeable. The WF operator seems to peak more often at higher pressures (600-750 hPa) in the dry regions than the J_{RH} operator (450-600 hPa), for instance over the Canary Islands (15ºW-25ºN) in winter and off the coast of Angola (5ºE-10ºS) in summer. For both seasons and in the moist regions associated to the ITCZ, the J_{RH} operator peaks on average at 250 hPa while the WF operator peaks lower, around 300 hPa.

We thus rely on this study for the choice of the vertical operator: in the following, the Free Tropospheric Humidity is defined as the mean relative humidity weighted by the relative humidity Jacobian J_{RH}. Indeed the use of J_{RH} gives the best interpretation of the layer of humidity observed by the 6.3 µm channel. In practice, the layer 150-700 hPa is considered in the computation of the FTH, using normalized weights:

$$FTH(RH) = \frac{\sum_{p=700hPa}^{150hPa} RH(p) \times J_{RH}(p)}{\sum_{p=700hPa}^{150hPa} J_{RH}(p)} \qquad (3)$$

with RH(p) scaling between 0 and 100%.

b) Impact of reanalysis

The impact of using a different reanalysis (here, ERA40 and ERA Interim) for the computation of the thermal parameter p0 is analysed because the CM SAF FTH software uses ERA Interim while LMD utilised ERA40 for p0 determination.

The Figure 6-3 presents an evaluation of the effect of the choice of the reanalysis on the computation of p0. Results shown here are estimated using model levels. Similar results are achieved if other vertical resolutions are considered (Roca et al., 2009).

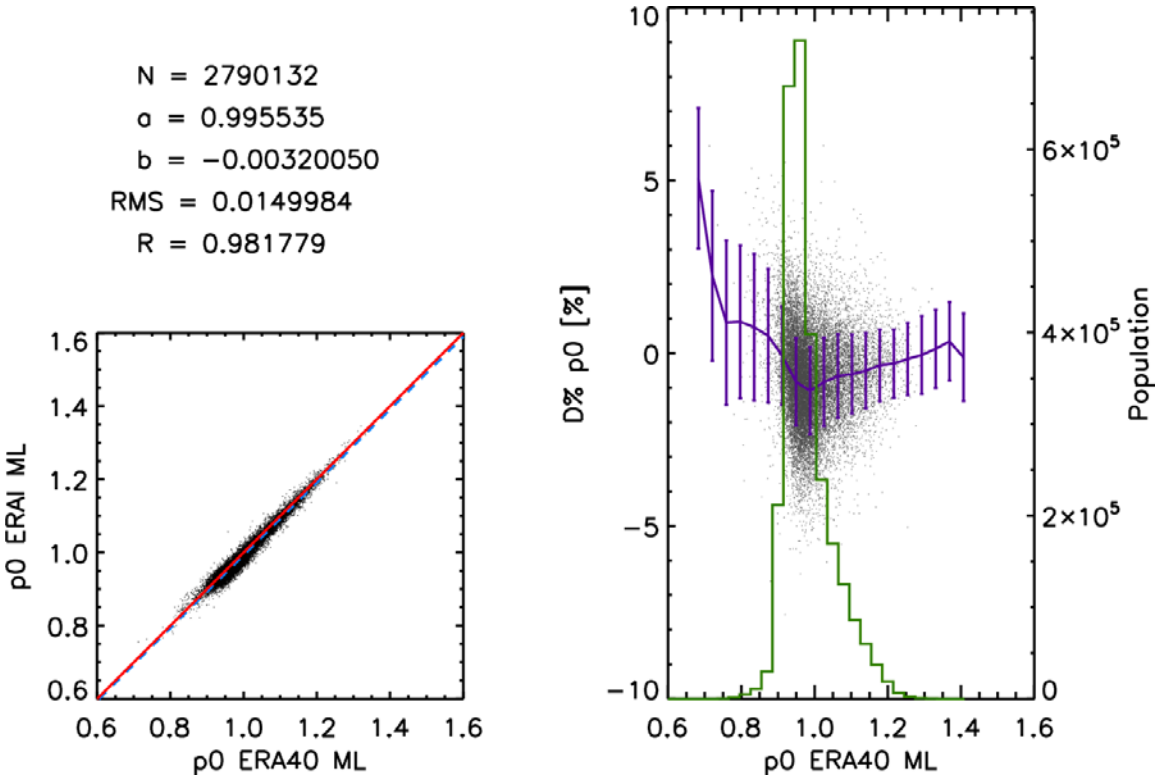

Figure 6-3*: Scatter plot of the p_0 computed from the ERA-40-ML versus the p_0 from the ERA-I-ML, with the x=y line (red) and the linear fit (dashed line). (b) Scatter plot of the relative differences $100 \times \Delta p_0/p_0$ (%) with the error bars computed in bins of 5% and the histogram of the population. The comparisons are performed from the temperature profiles of the whole year 2001.*

The effect of using a different reanalysis on the determination of p0 is small with a negligible bias of -0.003. Relative uncertainties are typically smaller than 4%. Such uncertainty translates into a 4% relative uncertainty in the estimation of FTH, all other things being equal, which indicates a non significant impact of the use of either the pressure level profiles or the model level profiles in the computation of p_0. In other words, the temperature profile didn't change largely in the free troposphere between ERA-40 and ERA-Interim. Therefore, the a priori information on the temperature profile needed for the application of the retrieval algorithm will not impact the quality of the retrieved FTH from the METEOSAT BTs.

c) Role of training data set

A number of geographical regions are used in the following to assess the sensitivity of the retrieval to the location of its training. Besides the general interest in the retrieval sensitivity on training area this analysis has also the objective to assess the applicability of the retrieval to full disc observations and the potential to define a single set of inversion coefficients valid for the nominal coverage and IODC. The considered training scenarios are summarized in Table 6-1. Note the 10-15% uncertainty from calibration (see section 5.2).

Table 6-1*: Summary of the geographical location.*

Name	Location	Number of profiles
Tropical Africa	45W-45E 30N-30S	22723
Tropical Indian Ocean	20W-110E 30N-30S	16925
Tropics	45W-110E 30N-30S	39648
Mid-latitudes	45W-45E 60N-40N	1227
Full disc	45W-45E 60N-60S	28421

Full disc training

The possibility of a full disc retrieval is now explored. A representative dataset is used for the training phase (Table 6-1). Figure 6-4 and Figure 6-5 show estimations of the quality of using these globally derived coefficients to compute FTH over the two sub-domains: mid-latitudes and Africa.

In the case of the application of the full disc retrieval coefficients, the results for the mid-latitudes profiles show that at the dry end of the spectrum of FTH, the relative bias can be larger than 10% and reaches 20% for the driest profiles. At the moist end, the bias remains bounded between 10 and 15%. The RMS is greater than 2%, the correlation is 0.96 and the mean relative bias is -1.63%. The full disc training is better suited for the African region where the statistics exhibits superior quality than over the mid-latitudes. Especially in the dry zones for which the relative bias is now well under 10%.

While a full disc retrieval computation yields a fit with high quality, its use may locally result in poorer scores. This is particularly true for the mid-latitudes. This result is rooted in the fact that the mid-latitude atmosphere cannot be easily apprehended with the present simplified UTH/FTH framework where the temperature profile is idealized (Ramond et al., 1981; Roca et al., 2009).

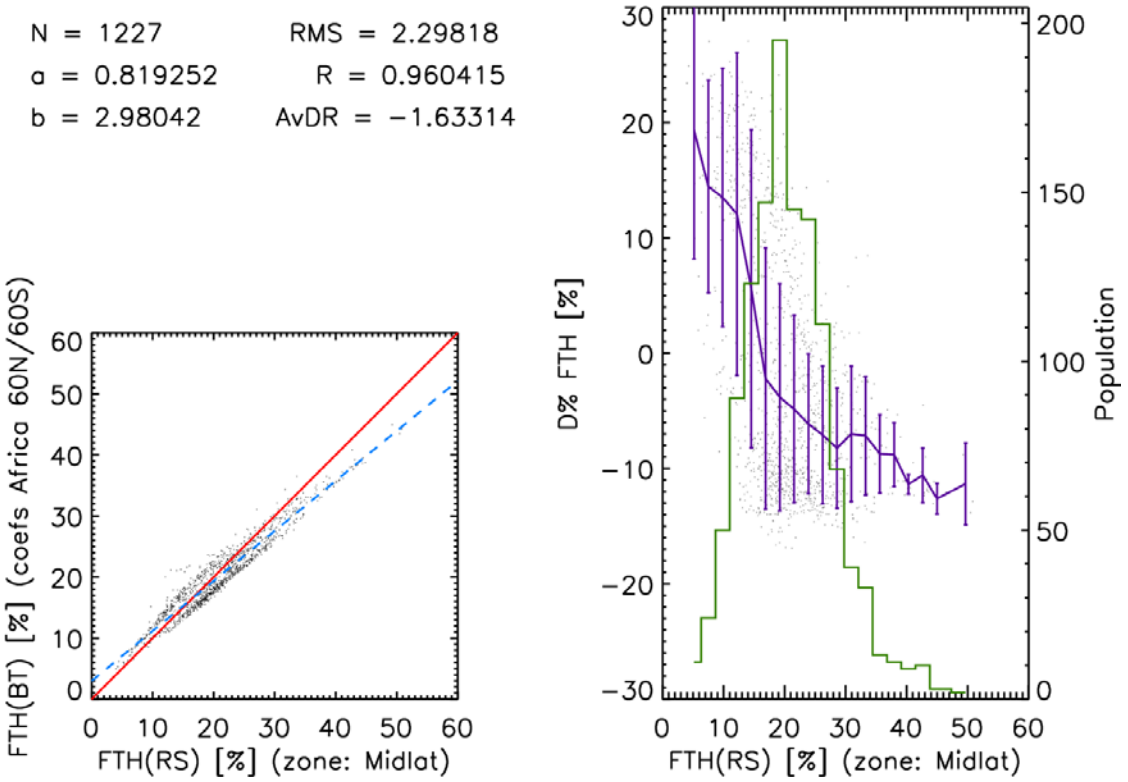

Figure 6-4*: (left) Scatter plot of FTH computed from the profile with the Jacobian versus FTH obtained from the BT and retrievals coefficients. (Right) Relative difference between the two as a function of the FTH computed from the profile with the Jacobian. Statistics for the mid-latitude profiles using full disc training.*

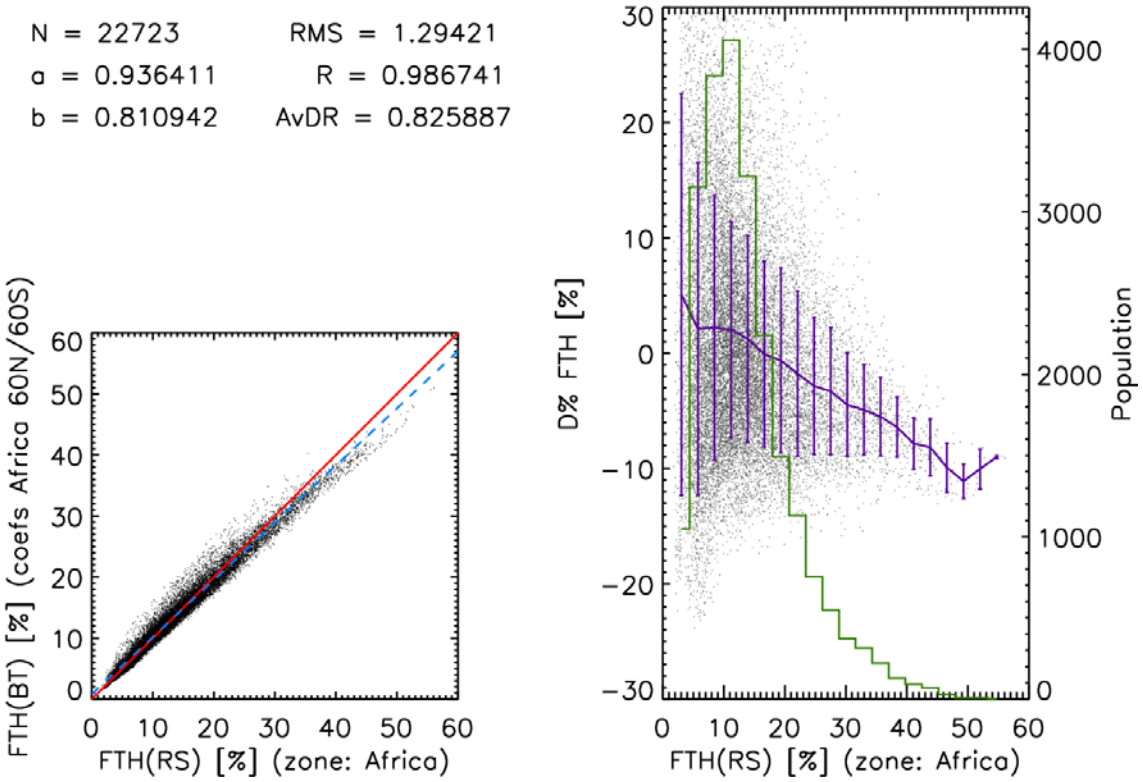

Figure 6-5*: Same as* Figure 6-4*. Scatter plots and statistics for the Africa region profiles using the full disc training.*

Africa/Atlantic vs. Indian Ocean vs. Tropics training

One of the aims of this work is to analyse the potential to apply a single retrieval scheme to nominal position and IODC data. To do so the retrieval (i.e. the a and b coefficients) developed for the Africa/tropical Atlantic (i.e. the nominal) coverage is evaluated against a retrieval based on training over IODC area. To complete this test, a third training database is composed of both nominal profiles and IODC profiles in order to have a database representative of the two areas. Figure 6-6 and Figure 6-7 represent the comparisons between the FTH estimated from the RH profiles (using J_{RH}) and the FTH retrieved from the BTs (and the fitting coefficients) using the African training datasets, applied to IODC and Tropics observations. These figures show the quality when extending the application to areas not covered by the training area.

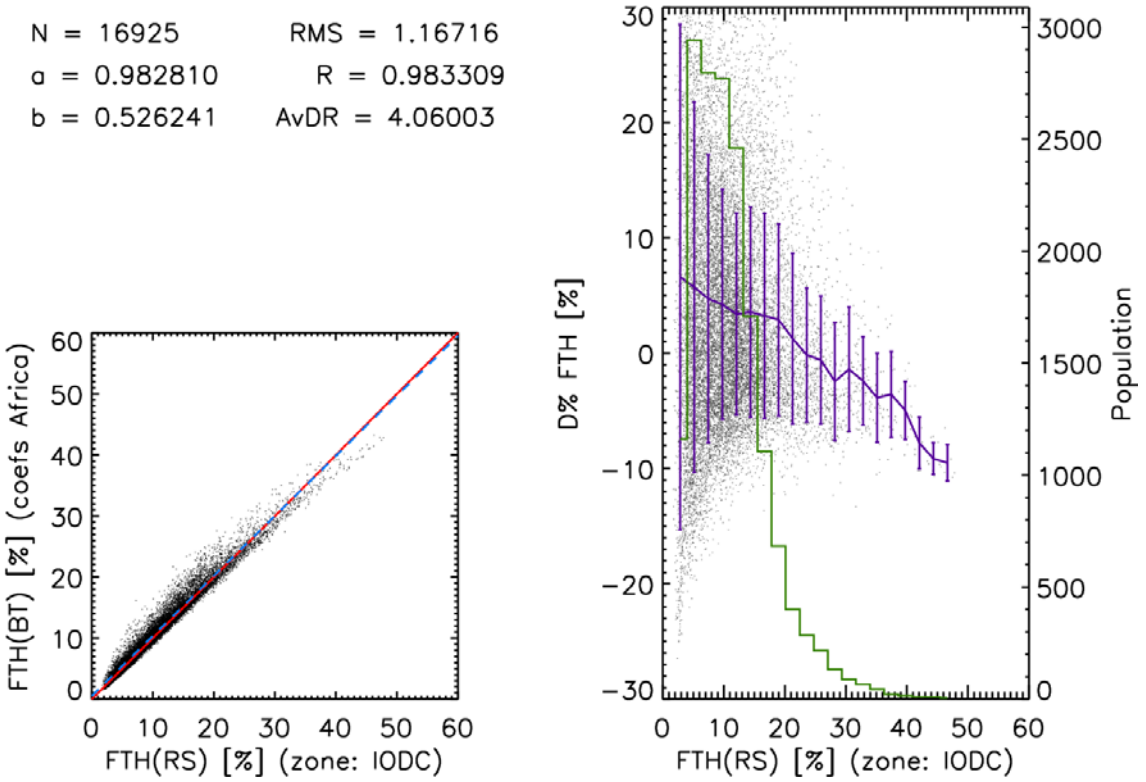

Figure 6-6*: Same as* Figure 6-4*. Scatter plots and statistics for the Indian Ocean region profiles using the training over Africa.*

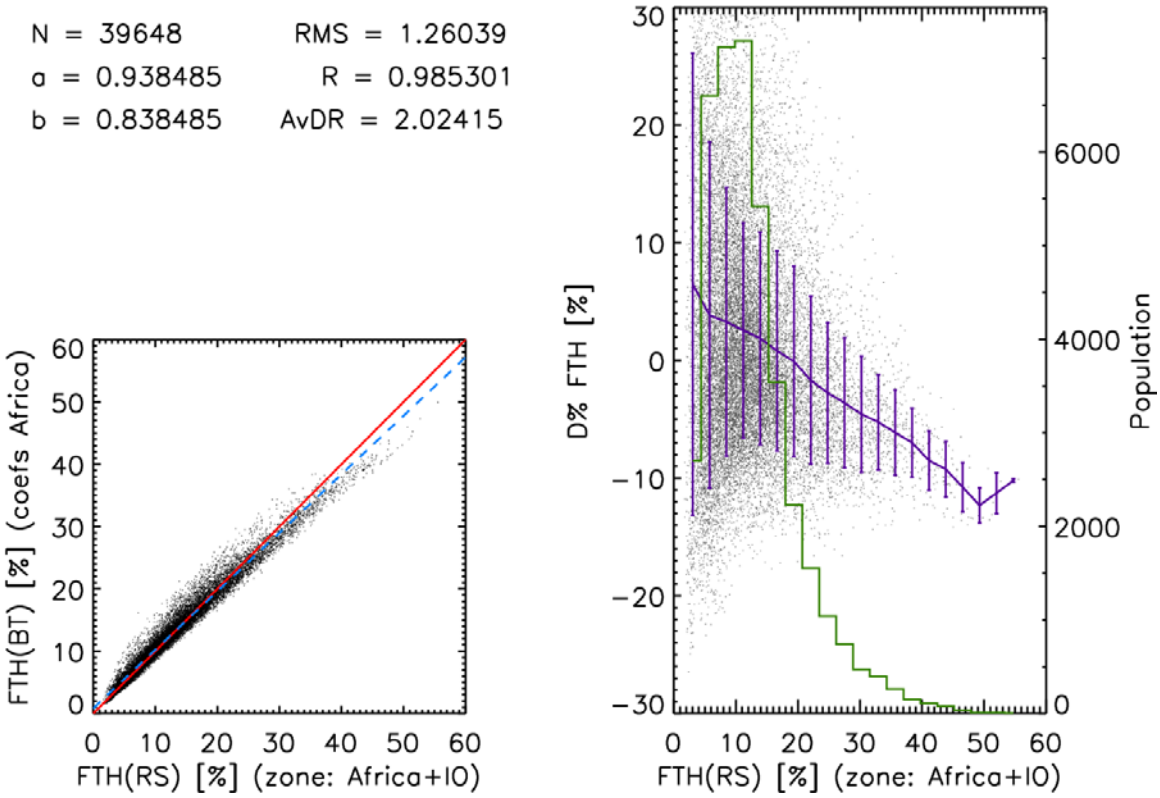

Figure 6-7*: Same as* Figure 6-6. *Scatter plots and statistics for the tropical region profiles using the African training.*

Figure 6-8 and Figure 6-9 show results for IODC and Tropics observations using coefficients from Tropics training. Here, the quality of Tropics training results is contrasted with quality achieved when applied to tropical subareas.

The four figures reveal a very similar picture in terms of quality and in particular they exhibit quality largely within expectations. Thus, a general (nominal coverage + IODC) set of retrieval coefficients can be applied to the Tropics but also to nominal coverage and IODC. It has the advantage that in principle the Tropics training includes more training cases and would allow an extension to IODC.

The implemented coefficients are: a=-0.1248 and b=33.46 from Tropics training using ERA-Interim with 60 model levels.

Further sensitivity analysis is given in Roca et al. (2009).

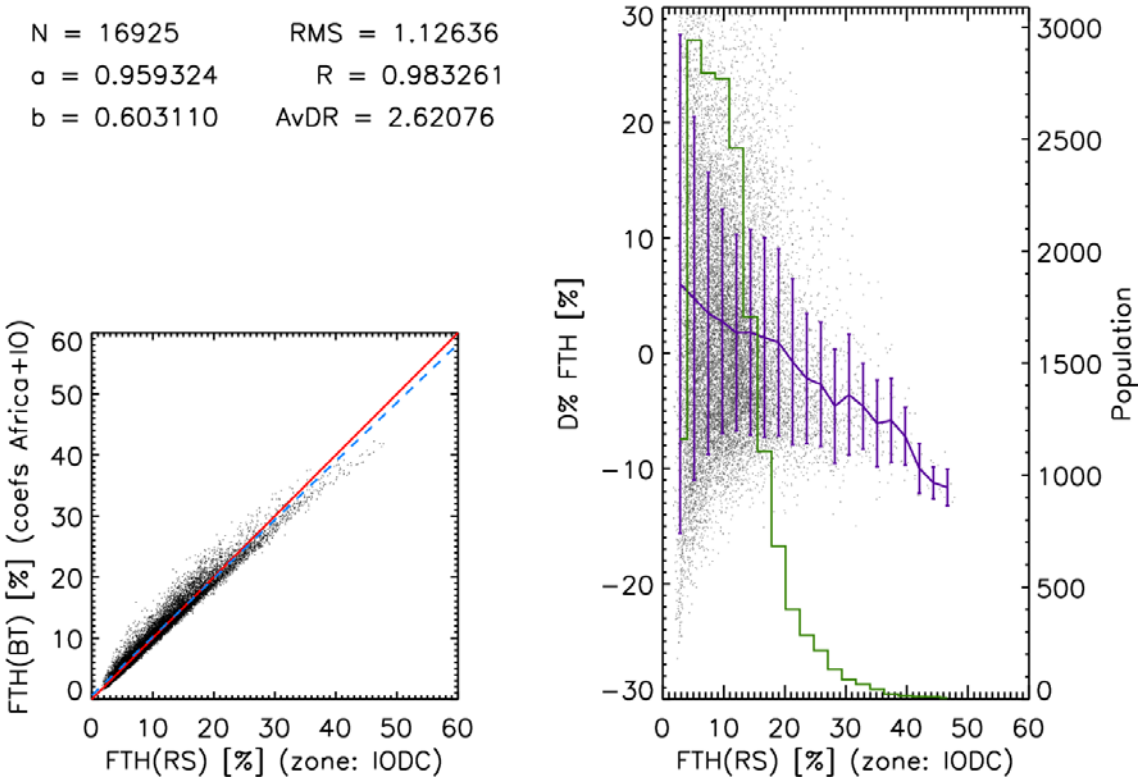

Figure 6-8: Same as Figure 6-6. Statistics for the Indian Ocean region using a training over the tropics (Africa+IO).

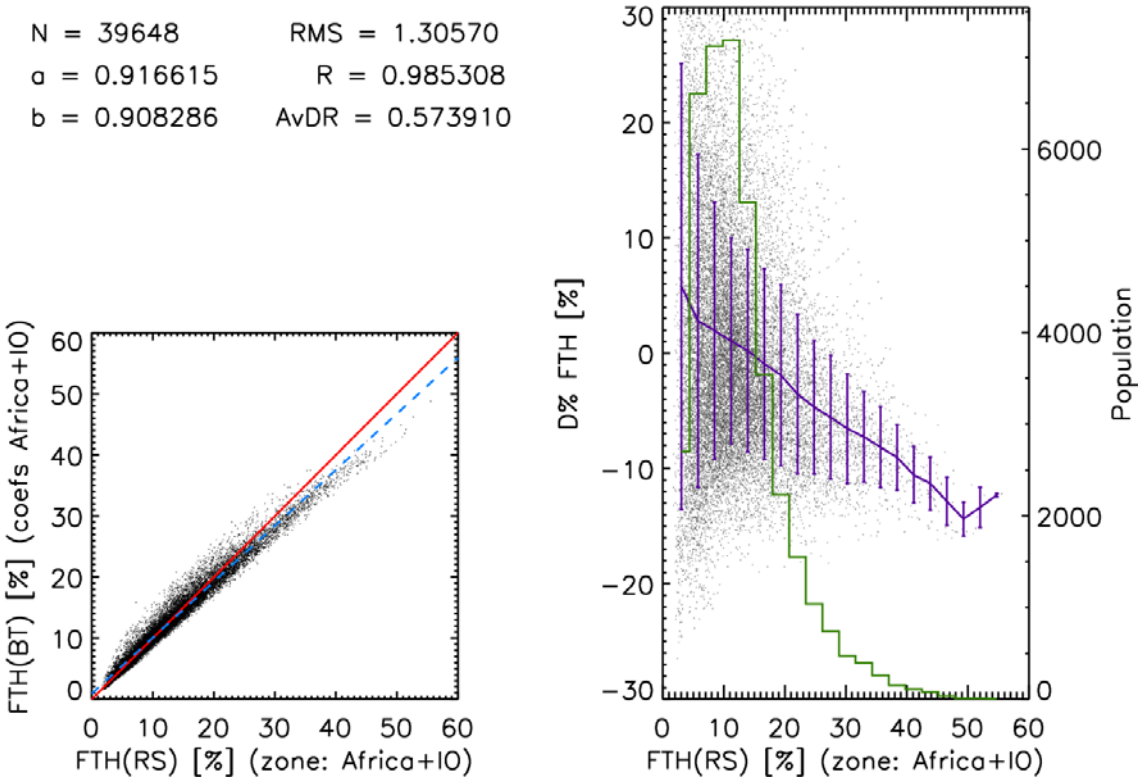

Figure 6-9: *Same as* Figure 6-6*. Scatter plots and statistics for the tropical region profiles using the tropical training.*

7 Assumptions and limitations

Though significant efforts have been dedicated to the homogenisation of the METEOSAT time series, the quality of the FTH retrieval would benefit from a recalibrated and intercalibrated FCDR for METEOSAT. The recovery of METEOSAT 6 data would close data gaps in the time series.

The identification of clear sky and low level clouds relies on ISCCP-DX data, and the FTH quality depends on the cloud classification quality. Strongest quality degradation can be expected when high level clouds are not correctly identified.

It could be shown that the quality of the retrieval decreases when applied to observations in mid-latitudes. Therefore, the application of the retrieval is restricted to the tropics, i.e., to an area within ±45°N/S and ±45°E/W.

The retrieval is not reliable over elevated terrain with surface pressures less than 700 hPa because the weighting function might reach the surface. Surface properties would then affect the observations for which the retrieval was not designed and which will degrade the quality of the FTH product.

8 References

Brogniez, H., African Free Tropospheric Humidity: Elaboration of a METEOSAT archive, Climatic analysis and Evaluation of models, PhD thesis, University of Pierre and Marie Curie, Paris, France, 2004.

Brogniez, H., R. Roca and L. Picon, Interannual and Intraseasonal variabilities of the Free Tropospheric Humidity using METEOSAT water vapor channel over the tropics, Proc. of the Eumetsat Meteorological Satellite Conference, Prague, Czech Rep, 31-4 June 2004.

Brogniez, H., R. Roca and L. Picon, A clear-sky radiance archive from Meteosat “water vapor” observations, J. Geophys. Res., 111, doi:10.10129/2006JD007238, 2006.

Buehler, S. A., and V. O. John (2005), A simple method to relate microwave radiances to upper tropospheric humidity, J. Geophys. Res., 110, D02110, doi:10.1029/2004JD005111.

Clough, S., Kneizys F. and R. Davies, Line shpae and the water vapor continuum, Atmos. Res., 23, 229-241, 1989.

Edwards, D, GENLN2: a general line-by-line atmospheric transmittance and radiance model, Tech. Rep., NCAR/TN-367, 1992.

Jackson, D. and J. Bates, Upper tropospheric humidity algorithm assessment, J. Geophys. Res., 106, 32,259-32,270, 2001.

Köpken, C. 2001: Monitoring of Meteosat WV radiances and solar stray light effects. EUMETSAT/ECMWF Fellowship Report No. 10.

Matricardi, M., F. Chevallier G. Kelly and J-N Thépaut, An improved general fast radiative transfer model for the assimilation of radiance observations, Quat. J. Roy. Meteor. Soc., 130, 153-173, 2004.

Picon, L., R. Roca, S. Serrar and M. Desbois, A new METEOSAT “water vapor” archive for climate studies, J. Geophys. Res., 108, doi: 10.1029/2002JD002640, 2003.

Roca, R., L. Picon, M. Desbois, H. Le Treut and J-J Morcrette, Direct comparison between METEOSAT water vapor channel and GCM results, Geophys. Res. Lett., 24, 147-150, 1997.

Roca R., H. Brogniez, L. Picon, and M. Desbois: Free Tropospheric humidity observations from Meteosat water vapour channel data. Preprints, 17th Conf. on Hydrology, Long Beach, CA, Amer. Meteor. Soc., CD-ROM, J3.7, 2003.

Roca, R., H. Brogniez, N. Gif and L. Picon: Development of a consistent climatology of free tropospheric humidity employing observations from METEOSAT satellites. EUMETSAT CM SAF Scientific and Technical Report, 23 October 2009.

Roca, R., Chambon, P., Jobard, I., Kirstetter, P.E. & Gosset, M. 2010. Comparing satellite and surface rainfall products over West Africa at meteorologically relevant scales during the AMMA campaign using error estimates. J. Appl. Meteor. Climatol., 49, 715–731.

Roca, R., H. Brogniez and L. Picon, A Free Tropospheric Humidity retrieval for METEOSAT water vapor channel, to be submitted to J. Geophys. Res., 2011.

Roca1, R., J. Meijer-Fofana, L. Picon1 and H. Brogniez: Climatology of free tropospheric humidity: Extension to SEVIRI, error analysis and trend assessment. EUMETSAT CM SAF Scientific and Technical Report, June 2012.

Rossow, W.B., and Schiffer, R.A., 1999: Advances in Understanding Clouds from ISCCP. Bull. Amer. Meteor. Soc., 80, 2261-2288.

Rothman, L. and co-authors, The HITRAN molecular spectroscopic database: edition of 2000 including updates through 2001, JQSRT, 82, 5-44, 2003.

Saunders, R., M. Matricardi, A. Geer, P. Rayer, O. Embury and C. Merchant, RTTOV-9 Science and validation report, Tech. Rep., ECMWF Satellite Application Facility on Numerical Weather Prediction, 2008.

Schmetz, J. and O. Turpeinen, Estimation of the upper tropospheric relative humidity field from METEOSAT water vapor image data, J. Appl. Meteor., 27, 889-899, 1988.

Schmetz, J., Operational calibration of the Meteosat water vapor channel by calculated radiances, Appl. Opt., 28, 3030-3038, 1989.

Schmetz, J., C. Geijo, W. P. Menzel, K. Strabala, L. van de Berg, K. Holmlund, and S. Tjemkes, 1995: Satellite observations of upper tropospheric relative humidity, clouds and wind field divergence. *Beitr. Phys. Atmos.,* 68, 345–357.

Shi, L., and J. J. Bates (2011), Three decades of intersatellite- calibrated High- Resolution Infrared Radiation Sounder upper tropospheric water vapor, J. Geophys. Res., 116, D04108, doi:10.1029/2010JD014847.

Soden, B. and F. Bretherton, Upper tropospheric relative humidity from the GOES 6.7µm channel : method and climatology for July 1987, J. Geophys. Res., 98, 16,669-16,688, 1993.

Soden, B. and F. Bretherton, Interpretation of TOVS water vapor radiances in terms of layer-average relative humidities: method and climatology for the upper, middle and lower troposphere, J. Geophys. Res., 101, 9333-9343, 1996.

Soden, B. and co-authors, An intercomparison of radiation codes for retrieving upper-tropospheric humidity in the 6.3µm band: a report from the first GvaP workshop, Bull. Am. Meteor. Soc., 81, 797-808, 2000.

Stephens, G., D. Jackson, and I. Wittmeyer, Global observations of upper tropospheric water vapor derived from TOVS radiance data, J. Climate, 9, 305-326, 1996.

Uppala, S. and co-authors, The ERA-40 re-analysis, Quart. J. Roy. Meteorol. Soc., 131, 2961-3012, 20.

van de Berg, L.C.J., J. Schmetz, and J. Whitlock, 1995: On the Calibration of the Meteosat Water Vapour Channel. J. Geophys. Res., 100, 21,069 (1995).

9 Glossary

ARSA	Analysed RadioSoundings Archive
ATBD	Algorithm Theoretical Baseline Document
AVHRR	Advanced Very High Resolution Radiometer
BT	Brightness Temperature
CDO	Climate Data Operators
CDOP	Continuous Development and Operations Phase
CM SAF	Satellite Application Facility on Climate Monitoring
CNRS	Centre national de la recherche scientifique
CSR	Clear Sky Radiance
DWD	Deutscher Wetterdienst (German MetService)
ECMWF	European Centre for Medium Range Forecast
ECV	Essential Climate Variable
EPS	European Polar System
EUMETSAT	European Organisation for the Exploitation of Meteorological Satellites
FCDR	Fundamental Climate Data Record
FMI	Finnish Meteorological Institute
FTH	Free Tropospheric Humidity
GCOS	Global Climate Observing System
GSICS	Global Space based Inter-Calibration System
IOP	Initial Operations Phase
ISCCP-DX	International Satellite Cloud Climatology Project, DX type
KNMI	Koninklijk Nederlands Meteorologisch Institut
LMD	Laboratoire Météorologie Dynamique
MVIRI	Meteosat Visible Infra-Red Imager
NetCDF	Network Common Data Format
NWP	Numerical Weather Prediction
PRD	Product Requirement Document
PUM	Product User Manual
RMIB	Royal Meteorological Institute of Belgium
RMSD	Root Mean Square Difference
SAF	Satellite Application Facility
SCOPE-CM	Sustained, Coordinated Processing of Environmental Satellite Data for Climate Monitoring
SEVIRI	Spinning Enhanced Visible and InfraRed Imager
SMHI	Swedish Meteorological and Hydrological Institute
WUI	Web User Interface